Research Paper submitted to Journal of the Electrochemical Society

Title:

Silicon Electrodeposition in a Water-soluble KF–KCl Molten Salt: Properties of Si Films on Graphite Substrates

Author Names:

Kouji Yasuda,[1,2,3, *, z] Tomonori Kato,[4] Yutaro Norikawa,[4] and Toshiyuki Nohira[4, *, z]

Affiliations:

[1] Department of Fundamental Energy Science, Graduate School of Energy Science, Kyoto University, Yoshida-honmachi, Sakyo-ku, Kyoto 606-8501, Japan.

[2] Agency for Health, Safety and Environment, Kyoto University, Yoshida-honmachi, Sakyo-ku, Kyoto 606-8501, Japan.

[3] Present address: Department of Materials Science and Engineering, Graduate School of Engineering, Kyoto University, Yoshida-honmachi, Sakyo-ku, Kyoto 606-8501, Japan.

[4] Institute of Advanced Energy, Kyoto University, Gokasho, Uji 611-0011, Japan.

* Electrochemistry Society Active Member

[z]Corresponding Author E-mail Addresses:

yasuda.kouji.3v@kyoto-u.ac.jp (K. Yasuda); nohira.toshiyuki.8r@kyoto-u.ac.jp (T. Nohira)

ORCID

Kouji Yasuda: https://orcid.org/0000-0001-5656-5359

Yutaro Norikawa: https://orcid.org/0000-0002-0861-5443

Toshiyuki Nohira: https://orcid.org/0000-0002-4053-554X

Abstract Text [200 Words or Less]

The electrodeposition of crystalline Si films on graphite substrates was investigated in KF–KCl molten salts at 1073 K. The optimum K_2SiF_6 concentration and current density to obtain adherent, compact, and smooth films were investigated using surface and cross-sectional scanning electron microscopy. The crystallinity of the deposited Si films was measured by X-ray diffraction and electron backscatter diffraction techniques. By photoelectrochemical measurements in CH_3CN–$TBAPF_6$–Fc at room temperature, the Si film electrodeposited on the graphite substrate at 100 mA cm^{-2} for 30 min in molten KF–KCl–K_2SiF_6 (3.5 mol%) was found to be an n-type semiconductor. When $SiCl_4$ was used as the Si source, the melt with a higher molar ratio of KF deposited smoother Si films on the graphite substrates. The Si films electrodeposited in molten KF–KCl after the introduction of $SiCl_4$ gas (2.37 mol%) were confirmed to be p-type by photoelectrochemical measurements in CH_3CN–$TBAClO_4$–$EVBr_2$. The characteristics of the electrodeposited Si film (p-type or n-type) is determined by the contaminating impurities (B, P, and Al).

Introduction

The installation of photovoltaic (PV) cells has increased drastically in the past two decades. The annual installation of PV cells exceeded 117 GW year^{-1} in 2019 [1]. PV cells are essential for transitioning to the renewable energy era in the near future. Crystalline Si solar cells are expected to continuously dominate the production share among various solar cell types because of their high efficiency, excellent stability, non-toxicity, and abundant natural resources. The major drawbacks of the current production method of Si substrates for PV cells are the significant kerf loss in the slicing step and low productivity of the Siemens process. Therefore, the development of a new alternative method for producing crystalline Si substrates is necessary.

The electrodeposition of crystalline Si has been proposed and reported as a candidate method for direct Si film formation on inexpensive solar cell substrates. Most studies on the electrodeposition of crystalline Si in high-temperature molten salts used all-fluoride molten salts such as LiF–KF and LiF–NaF–KF, with the aim of obtaining compact and smooth Si films [2–9]. The major problem regarding the use of all-fluoride molten salts is the low solubility of LiF in water, which makes it difficult to remove the adhered salt through water washing [8, 10]. In contrast, the problems associated with the use of all-chloride molten salts, such as NaCl–KCl and LiCl–KCl, are the poor smoothness of the deposits and the low solubility of Si(IV) ions in the melts [11–14].

The electrodeposition of crystalline Si in high-temperature molten salts has also been reported for fluoride–chloride mixed melts in several papers [15–24]. Andriiko *et al*. reported that the deposit obtained by adding K_2SiF_6 and SiO_2 to molten KF–KCl was in the powder form, with a Si composition of 20–50 wt% [15]. Kuznetsova *et al.* used NaCl–KCl–NaF molten salt and reported the diffusion coefficient of Si(IV) ions and the existence of a two-stage reduction of Si(IV) ions [16]. The same melt was also used by Zaykov *et al.*, who obtained fiber-like Si deposits and smooth Si films [21–23]. A recent work at MIT and the University of Texas reported the electrodeposition of smooth Si films from KF–KCl molten salts containing metallic Sn and K_2SiF_6 [24]. They measured the photoresponse of Sn-doped Si films formed on graphite substrates using linear sweep voltammetry in CH_3CN (acetonitrile)

containing 0.1 M $TBAPF_6$ (tetrabutylammonium hexafluorophosphate) and 0.05 M $Fe(C_5H_5)_2$ (Fc, ferrocene) under illumination of UV-vis light of 100 mW cm^{-2}. The Sn-doped Si exhibited n-type semiconductor behavior owing to the presence of a supervalent P dopant. Apart from the fluoride–chloride mixed melts, the semiconductor properties of the Si films deposited in $CaCl_2$-based molten salts were also measured using photoelectrochemical measurements [14, 25–27]. Photoelectrochemical measurements are useful for the preliminary evaluation of semiconductor properties because they can examine n-type or p-type characteristics without the formation of a p-n junction.

Our group also reported the electrochemical behavior of Si(IV) ions and obtained compact and smooth Si films on Ag substrates in molten KF–KCl after the addition of K_2SiF_6 or introduction of $SiCl_4$ gas at 923–1073 K [17–20]. Our proposed electrodeposition process for the formation of crystalline Si films uses a water-soluble KF–KCl molten salt as the electrolyte and $SiCl_4$ gas as the Si source. Si films are electrodeposited onto the cathode of an appropriate substrate, and Cl_2 gas is generated at the carbon anode.

$SiCl_4$ dissolution: $SiCl_4\ (g) + 6\ F^- \rightarrow SiF_6^{2-} + 4\ Cl^-$ (1)

Cathodic reaction: $SiF_6^{2-} + 4\ e^- \rightarrow Si\ (s) + 6\ F^-$ (2)

Anodic reaction: $4\ Cl^- \rightarrow 2\ Cl_2\ (g) + 4\ e^-$ (3)

Total reaction: $SiCl_4\ (g) \rightarrow Si\ (s) + 2\ Cl_2\ (g)$ (4)

The composition of the molten salt remains unchanged during the operation. Because the addition of K_2SiF_6 is easier than the introduction of $SiCl_4$ (reaction 1) to generate SiF_6^{2-} ions in the laboratory, several measurements were carried out using KF–KCl melts with the addition of K_2SiF_6 to investigate the effects of temperature, Si(IV) concentration, and current density [18, 20]. One of the advantages of the proposed process is the high solubility of the solidified KF–KCl salt in water, which enables the easy removal of the solidified salt adhering to Si deposits by water washing. The solubilities of KF and KCl are 101.7 g and 35.5 g, respectively, per 100 g of H_2O at 298 K, whereas the solubilities of LiF, NaF, MgF_2, and CaF_2 are 0.13, 4.15, 0.013, and 0.0016 g, respectively [28]. Another important point is the easy refinement of $SiCl_4$

via distillation. The evolved Cl_2 gas can be reused for the production of high-purity $SiCl_4$, and the construction of a closed-cycle production system is possible. However, to date, the effect of the substrate material on the electrodeposition of Si in KF–KCl molten salts has not been discussed. Moreover, the semiconductor properties have not been measured for any of the electrodeposited Si films prepared from the melts using K_2SiF_6 or $SiCl_4$ as Si sources.

In this study, we selected graphite as an inexpensive substrate material instead of Ag, which has previously been used. First, we investigated the optimum electrolysis conditions for obtaining compact and smooth Si films adhered to graphite substrates by varying the concentration of K_2SiF_6 in molten KF–KCl and the current density. Second, we investigated the conditions for obtaining compact and smooth Si films in molten KF–KCl after the introduction of $SiCl_4$. According to our previous study [19], when 2.30 mol% $SiCl_4$ was introduced into the eutectic KF–KCl, granular Si was obtained because the anion fraction of free F^- ions decreased upon the introduction of $SiCl_4$. Therefore, in the present study, we used a KF–KCl molten salt with a higher F^- ion concentration than the eutectic composition. Finally, from the future perspective of solar cell applications, photoelectrochemical measurements were performed to evaluate the semiconductor properties of the electrodeposited Si films.

Experimental

Electrochemical measurement and electrodeposition in molten KF–KCl

The experimental setup used has been described in another study [18]. The electrochemical experiments were conducted in a dry Ar glove box (Yamato Co., Ltd., ZYS15-0024) at 1073 K. Reagent-grade KF and KCl were mixed at the eutectic composition (KF:KCl = 45:55 mol%, melting point: 878 K [29]) or in the ratio KF:KCl = 60:40 mol% and loaded into a graphite crucible. The crucible was placed at the bottom of a stainless-steel vessel in an airtight Kanthal container and dried under vacuum at 773 K for 24 h. A graphite vessel was used instead of a stainless-steel vessel in the experiment to prevent metallic impurities from entering the system and enable the electrodeposition of high-purity Si. Prior to the relevant experiments, the crucible, vessel, and container were vacuum dried at 1073 K for 10 h to remove residual moisture. An Ar atmosphere was maintained during the experiments by passing Ar gas at a rate

of 50 mL min^{-1}. After blank measurements, a Si source was supplied to the melt either by the addition of K_2SiF_6 powder (Fuji Film Wako Pure Chemical Co., Ltd., >95%, Junsei Chemical Co., Ltd., >99%) or by the introduction of $SiCl_4$ gas via a vapor transport method, which is explained in the next section. A Ag flag (Nilaco Corp., 99.98%, diameter: 2.0 mm, thickness: 0.1 mm [17]) and a graphite plate (Toyo Tanso Co., Ltd., IG-15, width: 5.0 mm, thickness: 1.0 mm) were used as the working electrodes. A glassy carbon (GC) plate (Tokai Carbon Co., Ltd., width: 20 mm, thickness: 1.0 mm) was used as the counter electrode. A Si rod (Furuuchi Chemical Corp., 10N purity, diameter: 6.3 mm) was used as the counter electrode in the experiment, with an aim of electrodepositing high-purity Si. A Pt wire (Nilaco Corp., >99.98%, diameter: 1.0 mm) and a Si plate (p-type, resistivity: 9–12 Ω·cm, *ca*. 5 × 5 × 0.73 mm) were employed as the quasi-reference electrode and reference electrode, respectively. Because the consumption of Si(IV) ions during the Si electrodeposition experiments was less than 0.1% of the added Si ions, the Si electrode exhibited a stable Si(IV)/Si(0) potential. The potential of these reference electrodes was calibrated with reference to the dynamic K^+/K potential [17]. Galvanostatic electrolysis was conducted on the graphite substrates. The electrolyzed samples were washed in hot distilled water at 333 K for 24 h to remove the salt adhered to the deposits and dried under vacuum for 12 h. The samples were analyzed using scanning electron microscopy (SEM, Keyence Corp., VE-8800) and X-ray diffraction (XRD; Rigaku Corp., Ultima IV, Cu-Kα line). For the cross-sectional SEM observations, the samples were embedded in an acrylic resin and fabricated using a cross-section polisher with an Ar ion beam. The crystallinity was measured by field-emission scanning electron microscopy (FE-SEM; ZEISS, SUPRA35VP, or JEOL, JSM 7800F TSL) and electron backscatter diffraction (EBSD, ZEISS, SUPRA35VP + OIM5.31, SUPRA35VP + OIM6.2, or JEOL, JSM 7800F TSL + OIM7.1). The impurity concentrations in the Si deposits were analyzed by glow discharge mass spectrometry (GD-MS, Thermo Electron Corp., VG9000, or NU Instruments, Astrum).

Introduction of $SiCl_4$ gas into molten KF–KCl

The experimental setup used was described in a previous study [19]. Liquid $SiCl_4$ (Fuji Film Wako Pure Chemical Co., Ltd., >99.0%) held in a Pyrex bottle (100 mL) was maintained

in a water bath at 293 K using a thermostat (Scinics Corp., Cool Circulator CH-202). Perfluoroalkoxy alkane (PFA) tubes (outer diameter.: 6.35 mm, inner diameter: 4.35 mm) were attached to the screw cap (As-one, pipe diameter: 6–8 mm) of the bottle. The mixed Ar–$SiCl_4$ gas was prepared by bubbling Ar gas (30 mL min^{-1}, Kyoto Teisan, Inc., 99.999%) into liquid $SiCl_4$ using a PFA tube. The mixed gas was bubbled into molten KF–KCl (250 g of KF:KCl = 45:55 mol% or 400 g of KF:KCl = 60:40 mol%) at 1027 K using a graphite pipe (Toyo Tanso Co., Ltd., IG-11TS, outer diameter: 12 mm, inner diameter: 5 mm, length: 470 mm). After bubbling the mixed gas for a predetermined period, the lower end of the pipe was removed from the melt, and the flow gas was changed to pure Ar. Electrochemical measurements were then performed.

Photoelectrochemical measurement of Si films in organic solvent

Based on the reported methods [14, 24–27], photoelectrochemical measurements were performed using open-circuit potentiometry and linear sweep voltammetry at room temperature in an Ar atmosphere. The electrolyte was prepared by mixing $TBAClO_4$ (tetrabutylammonium perchlorate, 0.3 M, Sigma-Aldrich Co. LLC, >99%) and $EVBr_2$ (ethyl viologen dibromide, 0.05 M, Sigma-Aldrich Co. LLC, >99%) in CH_3CN (Fuji Film Wako Pure Chemical Co., Ltd., >95%), and the supernatant liquid in which $EV(ClO_4)_2$ (ethyl viologen diperchlorate) was dissolved was used as the electrolyte for the analysis of p-type Si. For the analysis of n-type Si, the electrolyte was prepared by mixing $TBAPF_6$ (0.1 M, Fuji Film Wako Pure Chemical Co., Ltd., >99.8%) and Fc (0.05 M, Fuji Film Wako Pure Chemical Co., Ltd., >98%) in CH_3CN. The electrolyte (15 mL) was placed in a glass beaker (50 mm × 25 mm × 50 mm), which was sealed with a rubber lid. The electrodeposited Si film was used as the working electrode after coating its edge with a masking agent (Taiyo Chemicals & Engineering Co. Ltd., Mask Ace S) and connecting it to a lead wire with a copper embossed conductive tape (Nitto Denko Corp., NITO Foil CT-311E). The surface area of the working electrodes was determined using image analysis software (ImageJ, National Institutes of Health, USA). A Pt wire (Tanaka Kikinzoku Kogyo K.K., 99.98%, diameter: 1.0 mm, immersion depth: *ca.* 10 mm) was used as the counter electrode. An Ag^+/Ag reference electrode was prepared by immersing a Ag wire (Tanaka

Kikinzoku Kogyo K.K., 99.99%, diameter: 1.0 mm) in a glass tube with a Vycor glass diaphragm containing $AgNO_3$ solution (0.01 M, Fuji Film Wako Pure Chemical Co., Ltd.). A Xe lamp (100 mW cm^{-2}) was used as the light source. The light was chopped at a frequency of 1 Hz during open-circuit potentiometry and linear sweep voltammetry.

Results and Discussion

Electrochemical measurement

The electrochemical behavior of Si (IV) ions was investigated by cyclic voltammetry in eutectic KF–KCl with 0.10 mol% K_2SiF_6 addition at 1073 K. Fig. 1(a) and 1(b) show the voltammograms obtained for the Ag flag and graphite electrodes, respectively. The voltammograms in the melt without K_2SiF_6 are also shown for reference. For the Ag electrode, reduction currents corresponding to Si deposition and K metal fog formation are observed from approximately 0.75 V and 0.35 V vs. K^+/K, respectively [20]. In the voltammogram for the graphite electrode, reduction currents are observed from 0.8 V in the negative scan and even in the blank melt. These currents may be due to the insertion of K into the graphite. After the addition of K_2SiF_6, larger reduction currents are observed than those in the blank melt. After the reversal of the sweep direction, anodic wave and shoulder are observed from approximately 0.75 V. To discuss the reduction behavior, the difference in the reduction current before and after the addition of 0.10 mol% K_2SiF_6 is plotted against the potential in Fig. 1(c). The reduction current starts at approximately 0.8 V and peaks at 0.53 V. Because the starting potential and shape of the voltammogram are similar to those of the Ag electrode in Fig. 1(a), it is concluded that the reduction current corresponds to the electrodeposition of Si. As described above, the starting potentials for Si deposition and K insertion at the graphite electrode are both almost 0.8 V. Since these reactions tend to occur simultaneously, it is necessary to conduct electrodeposition under conditions where the K insertion reaction is suppressed.

*** Fig. 1 ***

Optimization of electrodeposition conditions

The optimum conditions for the electrodeposition of adherent, compact, and smooth Si layers on graphite substrates were investigated in molten KF–KCl–K_2SiF_6 at 1073 K. Galvanostatic electrolysis for Si deposition was conducted with a charge density of 180 C cm^{-2} at 0.50 to 5.0 mol% K_2SiF_6 and a cathodic current density of 25 to 400 mA cm^{-2}. Photographs of the obtained samples are presented in Fig. S1, where electrolysis was not performed under shaded conditions in the frame. Gray or black films were deposited under all the electrolysis conditions. At high current densities, the electrodeposits were concentrated at the edge of the plate electrode.

Surface SEM images of typical samples are shown in Fig. 2 (surface SEM images of all samples are shown in Fig. S2). At the same K_2SiF_6 concentration, in the sample electrolyzed at a high current density, the deposit is porous with fine holes. In contrast, the sample at a low current density of 25 mA cm^{-2} shows voids between the electrodeposits. The morphologies of the electrodeposited Si films were evaluated in detail using cross-sectional SEM observations. Figure 3 shows cross-sectional SEM images of typical samples (cross-sectional SEM images of all samples are shown in Fig. S3). Adherent, compact, and smooth Si films with a thickness of approximately 30 μm are observed under the conditions of 2.0–5.0 mol% K_2SiF_6 concentration and 50–100 mA cm^{-2} current density.

Based on the SEM images presented in Figs. 3 and S3, the relationship between the electrolysis conditions and the morphology of the Si deposits is shown in Fig. 4 (the stars indicate the experimental electrolysis conditions). Outside the range of optimum electrolysis conditions, the morphology of the deposited Si film is not smooth because of the following reasons. At a high current density, the morphology of the Si film changes to porous and nodular. Although a higher current density results in a higher nucleation density, the smoothness of the film is reduced due to the larger growth rate. Electrolysis at a high current density also increases the concentration gradient of Si ions in the diffusion layer, resulting in their preferential deposition on the convex parts of the grown edge of the deposited Si. This phenomenon has already been confirmed at 923 K using an Ag substrate [18]. Another aspect of the morphology of Si deposits is the insertion of K into graphite. In the case of the graphite substrate, the

insertion reaction of K may occur simultaneously, especially at high current densities. The volume expansion of graphite due to K insertion may have reduced the smoothness of the substrate and caused the nodularization of the Si film. Incidentally, the potentials during the electrolysis at 400 mA cm^{-2} and 100 mA cm^{-2} in 3.5 mol% K_2SiF_6 concentration were 0.52 V and 0.64 V, respectively, at which K metal fog formation does not occur. At very low current densities, the thickness of the Si layer becomes non-uniform. This may be owing to the low nucleation density caused by the insufficient overvoltage and/or non-uniform current distribution on the electrode. For comparison, the reported optimum electrolysis conditions for the Ag substrate at 1073 K are also shown in Fig. 4 [20]. The optimum conditions for the graphite substrate exist at a lower current density than that for Ag substrate (2.0–3.5 mol% K_2SiF_6 and 100–300 mA cm^{-2}).

*** Fig. 2 ***

*** Fig. 3 ***

*** Fig. 4 ***

Characterization of Si film obtained from K_2SiF_6-added melt

To evaluate the semiconductor properties of the deposited Si films, 3.5 mol% K_2SiF_6 and 100 mA cm^{-2} was selected as the sample preparation condition for photoelectrochemical measurements. Prior to the photoelectrochemical measurements, the sample was analyzed by XRD, SEM, EBSD, and GD-MS.

Figure 5(a) shows the XRD pattern, in which only the peaks attributed to Si and graphite are observed. The crystallite size evaluated according to the Scherrer equation [30] and the full width at half maximum (FWHM) of the 220 diffraction peak was over 100 nm.

$$D = \frac{K\lambda}{\beta \cos\theta} \tag{5}$$

Here, D is the crystallite size, K is the Scherrer constant (0.94), λ is the wavelength (0.15418

nm), β is the FWHM, and θ is the Bragg angle.

Figure 5(b) shows a magnified view of the cross-sectional SEM image in Figure 3. The deposition of an adherent, compact, and smooth Si film with a thickness of approximately 30 μm is reconfirmed. The electrodeposits were further measured using cross-sectional EBSD analysis. Figure 5(c) shows a crystal grain map of the Si deposits. In the map, the crystal orientation is indicated by color, as shown in the inverse pole figure, and the crystallite size is indicated based on the area using a particular color. Very fine grains and a crystal grain boundary are indicated in black. The analysis clarifies that the crystals are generally fine, and that the grain boundaries or very small grains shown in black are abundant. The crystallites of the Si deposit obtained on the graphite substrate at 100 mA cm^{-2} are small with respect to those on the Ag substrate (15 × 30 μm in columnar shape [20]). The main reason for this may be that the graphite substrate is less oriented and has smaller crystallites than the Ag substrate, and thus smaller crystals were deposited reflecting such substrate conditions.

Table 1 summarizes the GD-MS results for the deposited Si films. For comparison, the table also lists the reported acceptable impurity levels for solar-grade Si (SOG-Si) [31–34] and the purity of the Si films obtained on Ag substrates in our previous study [18]. In the Si film obtained from the K_2SiF_6-added melt, the total amount of impurities was 35 ppm. Although some impurity elements exceeded their acceptable impurity levels, the following three experimental improvements suppressed the occurrence of metallic impurities compared to the previously prepared Si film on the Ag substrate: (1) use of high-purity chemicals (KF: 99%, KCl: 99.5%, and K_2SiF_6: 99%), (2) use of a graphite vessel instead of a stainless-steel vessel to prevent metallic impurities, and (3) use of a Si anode to prevent metal corrosion by evolved Cl_2 gas. Nevertheless, in order to develop a closed-cycle production system that uses the evolved Cl_2 gas (reaction (3)) to produce $SiCl_4$, it is necessary to achieve higher purity even with carbon anodes.

Photoelectrochemical measurements of the above deposited Si film were carried out using open-circuit potentiometry and linear sweep voltammetry in a CH_3CN–$TBAPF_6$ electrolyte containing an Fc reducing agent. Photographs of the sample before and after preparation for the photoelectrochemical measurements are shown in Fig. S4. As shown in Fig. 6(a), the open-

circiut potentil is −0.1 V vs. Ag^+/Ag in the dark. When the light illumination was chopped, potential changes up to approximately −0.38 V are observed during the illumination. The negative potential shift under illumination is owing to the diffusion of holes generated in the valence band to the electrode surface, indicating that the deposited Si is an n-type semiconductor. In the linear sweep voltammogram, the oxidation dark current gradually increases from the open circuit potential to 0.7 V at a maximum of 2 mA cm^{-2}, as shown by the blue line in Fig. 6(b). The voltammogram under illumination was also measured from the open-circuit potential in the dark (approximately −0.1 V). As shown by the red line, the oxidation photocurrent is already observed at −0.1 V. During the potential sweep, stepwise currents are observed corresponding to the chopping of the light, as shown by the green line. The oxidation photocurrent, which is larger than the dark current, indicates the existence of photoexcited holes, which also confirms that the electrodeposited Si film is an n-type semiconductor.

$$Fc + h^+ \rightarrow Fc^+ \qquad (6)$$

Considering the analysis results in Table 1, the contamination of P impurity is regarded as the reason for the n-type characteristics. Though the existence of dark current means that some degree of impurities are present in the Si film, the confirmation of n-type characteristics by photocurrent is an achievement for an initial experiment.

*** Fig. 5 ***

*** Table 1 ***

*** Fig. 6 ***

Characterization of Si film obtained from $SiCl_4$-introduced melt

Following the suggestion in our previous work on eutectic KF–KCl (45:55 mol%) [19], we also used a KF–KCl melt with a higher molar ratio of KF. The composition of KF:KCl = 60:40 mol% was selected so that the supply of 3.0 mol% $SiCl_4$ provides the same anionic

fraction of F^- and Cl^- ions as the eutectic KF–KCl after the addition of 3.0 mol% K_2SiF_6. In this study, both the eutectic KF–KCl and 60mol%KF–40mol%KCl were used as the initial melts, and electrochemical measurements and electrodeposition were performed after the introduction of $SiCl_4$.

For the eutectic KF–KCl, 19.14 g of $SiCl_4$ gas was supplied at 1073 K by the gas transport method. The Si(IV) ion concentration was 2.79 mol% and the dissolution efficiency was 95%, which was estimated by cyclic voltammetry using an Ag electrode. The Si films were electrodeposited at 100 mA cm^{-2} for 30 min. The surface SEM image (Fig. 7(a-1)) shows that the film is bumpy and not smooth. The formation of a bumpy Si film is also confirmed by cross-sectional SEM at the center of the substrate, as shown in Fig. 7(a-2). The thickness of 20–30 μm is smaller than the theoretical value of 56 μm, indicating that deposition preferentially occurred at the edges.

In the case of 60mol%KF–40mol%KCl, the Si(IV) ion concentration was 2.37 mol%, which was confirmed by cyclic voltammetry. The surface and cross-sectional SEM images of the Si film obtained at 45.6 mA cm^{-2} for 60 min are shown in Figs. 7(b-1) and 7(b-2), respectively. The deposition of a compact and smooth film with a thickness of approximately 50 μm is confirmed. Because the value is almost the same as the theoretical thickness of 51 μm, it is confirmed that preferential deposition did not occur at the edges. In summary, the use of molten KF–KCl with a high F^- ion concentration is the key to electrodeposit compact and smooth Si films from the melt after the introduction of $SiCl_4$.

The results of the purity analysis using GD-MS are shown in Table 1. The detected K is attributed to residual salt on the surface, or K electrochemically inserted into the graphite substrate diffused to the deposited Si. The total impurity content, except for K, is less than 100 ppm. Notably, although the purity of Si (4N, 99.99%) does not reach that of the solar-grade Si (6N, 99.9999%), the concentration of metal impurities, excluding Al, does not exceed 1 ppm. The contamination of B and P is probably due to the presence of a graphite vessel or crucible. Diffusion from the graphite substrate is also a candidate cause of contamination.

Photoelectrochemical measurements of the above deposited Si films were carried out in CH_3CN–$TBAClO_4$ (0.3 M) containing an EV^{2+} (0.05 M) oxidizing agent. The linear sweep

voltammograms obtained without the chopper are shown in Fig. 8. While the reduction dark current starts at approximately −0.7 V, the reduction photocurrent at approximately −0.5 V.

$$EV^{2+} + e^{-} \rightarrow EV^{+} \quad (7)$$

The reduction photocurrent, which is larger than the dark current, indicates the existence of photoexcited electrons, confirming that the electrodeposited Si film is a p-type semiconductor. The p-type semiconductor characteristics of the electrodeposited Si films are different from those of the Si films prepared in the KF–KCl–K_2SiF_6 melt (Fig. 6). The main reason for the p-type characteristics may be the inclusion of B and Al impurities (B: 23 ppm, Al: 12 ppm, P: 12 ppm, see Table 1).

Throughout the series of experiments, compact and smooth Si films were obtained using $SiCl_4$ as the Si source in KF–KCl with a high F^- ion concentration. The electrodeposited Si exhibited the characteristics of a p-type semiconductor. Although the control of the p/n semiconductor characteristics was not achieved at this time, the possibility of applying the proposed process to the production of solar cell substrates was clarified. The fact that the photocurrent of the Si deposited film from KF–KCl–$SiCl_4$-added melt was smaller than that of the deposited Si film obtained from the K_2SiF_6-added melt suggests that the semiconducting properties of the Si film were inferior; therefore, efforts are required to improve the purity. In the future, we shall study the optimum electrolysis conditions, such as anion fraction, Si(IV) ion concentration, and current density, to obtain Si films with higher quality for PV applications.

*** Fig. 7 ***

*** Fig. 8 ***

Conclusions

The electrodeposition of Si onto graphite substrates from KF–KCl–K_2SiF_6 and KF–KCl–$SiCl_4$ molten salts was investigated at 1073 K. The optimum electrolysis conditions to obtain adherent, compact, and smooth Si films were found to be 2.0–5.0 mol% K_2SiF_6

concentrations and 50–100 mA cm^{-2} current densities. While the optimum condition range for the K_2SiF_6 concentration for the graphite substrate was almost the same as that for the Ag substrate, it was lower than that for the Ag substrate for the current density. The Si crystallites formed on the graphite substrate were generally fine. The purity of Si films electrodeposited in KF–KCl–K_2SiF_6 and KF–KCl–$SiCl_4$ molten salts was almost 4N in both cases. The inclusion of metal impurities was suppressed by using high-purity chemicals, a graphite vessel, and a Si anode. The morphology of the Si film was improved by using KF–KCl with a high F^- ion concentration as the bath for introducing $SiCl_4$. The Si films prepared in KF–KCl–K_2SiF_6 and KF–KCl–$SiCl_4$ molten salts exhibited n-type and p-type semiconductor characteristics in photoelectrochemical measurements, respectively.

Acknowledgments

This study was partly supported by a Grant-in-Aid for Scientific Research A (Grant Number 16H02410 and 21H04620) from the Japan Society for the Promotion of Science (JSPS). EBSD measurements were performed at Sumitomo Electric Industries, Ltd.

References

1. International Renewable Energy Agency (IRENA), Report "Future of Solar Photovoltaic", (2019). https://www.irena.org/publications/2019/Nov/Future-of-Solar-Photovoltaic
2. U. Cohen and R. A. Huggins, *J. Electrochem.*, **123**, 381 (1976).
3. G. M. Rao, D. Elwell, and R. S. Feigelson, *J. Electrochem. Soc.*, **128**, 1708 (1981).
4. D. Elwell and R. S. Feigelson, *Sol. Energy, Mat.*, **6**, 123 (1982).
5. G. M. Rao, D. Elwell, and R. S. Feigelson, *J. Electrochem. Soc.*, **127**, 1940 (1980).
6. K. S. Osen, A. M. Martinez, S. Rolseth, H. Gudbrandsen, M. Juel, and G. M. Haarberg, *ECS Trans.*, **33**, 429 (2010).
7. A. L. Bieber, L. Massot, M. Gibilaro, L. Cassayre, P. Taxil, and P. Chamelot, *Electrochim. Acta*, **62**, 282 (2012).
8. G. M. Haarberg, L. Famiyeh, A. M. Martinez, and K. S. Osen, *Electrochim. Acta*, **100**, 226 (2013).
9. Y. Sakanaka and T. Goto, *Electrochim. Acta*, **164**, 139 (2015).
10. J. Xu and G. M. Haarberg, *High Temp. Mater. Processes (De Gruyter)*, **32**, 97 (2013).
11. R. Boen and J. Bouteillon, *J. App. Electrochem.*, **13**, 277 (1983).
12. T. Matsuda, S. Nakamura, K. Ide, K. Nyudo, S. Yae and Y. Nakato, *Chem Lett.*, **7**, 569 (1996).
13. S. V. Devyatkin, *J. Min. Metall. Sect. B.*, **39**, 303 (2003).
14. J. Zhao, H. Yin, T. Lim, H. Xie, H. Y. Hsu, F. Forouzan, and A. J. Bard, *J. Electrochem. Soc.*, **163**, 506 (2016).
15. A. A. Andriiko, E. V. Panov, O. I. Boiko, B. V. Yakovlev, and O. Y. Borovik, *Russ. J. Electrochem.*, **33**, 1343 (1997).
16. S. V. Kuznetsova, V. S. Dolmatov, and S. A. Kuznestov, *Russ. J. Electrochem.*, **45**, 797 (2009).
17. K. Maeda, K. Yasuda, T. Nohira, R. Hagiwara, and T. Homma, *J. Electrochem. Soc.*, **162**, D444 (2015).
18. K. Yasuda, K. Maeda, T. Nohira, R. Hagiwara, and T. Homma, *J. Electrochem. Soc.*, **163**, D95 (2016).
19. K. Yasuda, K. Maeda, R. Hagiwara, T. Homma, and T. Nohira, *J. Electrochem. Soc.*, **164**, D67 (2017).
20. K. Yasuda, K. Saeki, T. Kato, R. Hagiwara, and T. Nohira, *J. Electrochem. Soc.*, **165**, D825 (2018).
21. Y. P. Zaykov, S. I. Zhuk, A. V. Isakov, O. V. Grishenkova, and V. A. Isaev, *J. Solid State Electrochem.*, **19**, 1341 (2015).
22. S. I. Zhuk, A. V. Isakov, A. P. Apisarov, O. V. Grishenkova, V. A. Isaev, E. G. Vovkotrub, and Y. P. Zaykov, *J. Electrochem. Soc.* **164**, H5135 (2017).
23. S. I. Zhuk, V. A. Isaev, O. V. Grishenkova, A. V. Isakov, A. P. Apisarov, and Y. P. Zaykov, *J. Serb. Chem. Soc.*, **82**, 51 (2017).
24. J. Peng, H. Yin, J. Zhao, X. Yang, A. J. Bard, and D. R. Sadoway, *Adv. Funct. Mater.*, 1703551 (2017).
25. X. Yang, L. Ji, X. Zou, T. Lim, J. Zhao, E. T. Yu, and A. J. Bard, *Angew. Chem. Int. Ed.*

56, 15078 (2017).
26. X. Zou, L. Ji, X. Yang, T. Lim, E. T. Yu, and A. J. Bard, *J. Am. Chem. Soc*., **139**, 16060 (2017).
27. X. Zou, L Ji, J. Ge, D. R. Sadoway, E. T. Yu, and A. J. Bard, *Nat. Commun.*, **10**, 5772 (2019).
28. J. R. Rumble, *CRC Handbook of Chemistry and Physics, 99th Edition* (2018).
29. L. P. Cook and H. F. McMurdie, *Phase Diagrams for Ceramists vol. VII*, p. 509, The American Ceramic Society Inc., Columbus (1989).
30. B. D. Cullity, Agne Shofusha, Tokyo, *Elements of X-Ray Diffraction, 2nd edition* (2002).
31. Y. Kato, N. Yuge, S. Hisawa, H. Terashima, and F. Aratani, *Materia Japan*, **41**, 54 (2002).
32. M. A. Martorano, J. B. F. Neto, T. S. Oliveira, and T. O. Tsubaki, *Mater. Sci. Eng. B*, **176**, 217 (2011).
33. R. H. Hopkins and A. Rohatgi, *J. Crystal Growth*, **75**, 67 (1986).
34. J. R. Davis, Jr., A. Rohatgi, R. H. Hopkins, P. D. Blais, P. Rai-Choudhury, J. R. McCormick, and H. C. Mollenkopf, *IEEE Trans. Electron Devices*, **27**, 677 (1980).

Figure Captions

Fig. 1 Cyclic voltammograms at (a) a Ag flag electrode and (b) a graphite plate electrode in molten KF–KCl before and after addition of K_2SiF_6 (0.10 mol%) at 1073 K. Scan rate: 0.50 V s^{-1}. (c) Current–potential curve calculated from the difference for the voltammograms obtained at a graphite plate electrode in blank melt and molten KF–KCl−K_2SiF_6 (0.10 mol%).

Fig. 2 Surface SEM images of the samples obtained by galvanostatic electrolysis of graphite plate electrodes at various current densities and K_2SiF_6 concentrations in molten KF–KCl at 1073 K. The charge density was at 180 C cm^{-2}.

Fig. 3 Cross-sectional SEM images of the samples obtained by galvanostatic electrolysis of graphite plate electrodes at various current densities and K_2SiF_6 concentrations in molten KF–KCl at 1073 K. The charge density was 180 C cm^{-2}.

Fig. 4 Relationship between electrolysis conditions and morphology of Si deposits on graphite electrode and the optimum electrolysis conditions for Ag substrate [20].

Fig. 5 (a) XRD pattern, (b) cross-sectional SEM image, and (c) a crystal grain map from electron backscatter diffraction (EBSD) analysis of the deposits obtained by galvanostatic electrolysis of a graphite plate electrode at 100 mA cm^{-2} for 30 min in molten KF–KCl–K_2SiF_6 (3.5 mol%) at 1073 K.

Fig. 6 (a) Open-circuit potentiogram and (b) linear sweep voltammograms at an electrodeposited Si in CH_3CN–$TBAPF_6$(0.1 M)–Fc(0.05 M) at room temperature. Scan rate: 0.05 V s^{-1}.

Fig. 7 Surface and cross-sectional SEM image of the samples obtained by galvanostatic electrolysis of graphite plate electrodes. The Si layer was electrodeposited (a-1)(a-2) at 100 mA cm^{-2} for 30 min in molten KF–KCl (45:55 mol%) at 1073 K after the introduction of $SiCl_4$ (2.79mol%) and (b-1)(b-2) at 45.6 mA cm^{-2} for 60 min in molten KF–KCl (60:40 mol%) at 1073 K after the introduction of $SiCl_4$ (2.37 mol%).

Fig. 8 Linear sweep voltammograms at the electrodeposited Si in CH_3CN–$TBAClO_4$ (0.3 M)–$EVBr_2$ (0.05 M) at room temperature. Scan rate: 0.05 V s^{-1}.

Table 1 Acceptable impurity levels for SOG-Si [31–34] and impurity contents determined by GD-MS for the Si film samples. The samples were obtained by galvanostatic electrolysis of a Ag plate at 100 mA cm^{-2} for 50 min in molten KF–KCl–K_2SiF_6 (2.0 mol%) at 923 K [18], a graphite plate at 100 mA cm^{-2} for 30 min in molten KF–KCl–K_2SiF_6 (3.5 mol%) at 1073 K, and a graphite plate at 45.6 mA cm^{-2} for 60 min in molten KF–KCl at 1073 K after the introduction of 2.37 mol% $SiCl_4$.

Element	Acceptable levels for SOG-Si / ppm			Impurity content in electrodeposited Si film / ppm		
	[31]	[32]	[33, 34]	Ag plate (GC rod anode) [18]	Graphite plate (Si rod anode) [This study]	Graphite plate (GC plate anode) [This study]
				K_2SiF_6	K_2SiF_6	$SiCl_4$
B	0.1–0.3	0.1–10	—	3.2	< 1	23
Al	< 0.06	0.005–0.05	—	0.8	5	12
P	< 0.1	0.02–2	—	2.7	11	12
K	—	—	—	< 2	10	78
Ca	—	< 2	—	< 1	< 1	1.0
Ti	$< 4\times10^{-5}$	< 1	$< 1\times10^{-4}$	< 0.1	< 1	0.13
Cr	—	—	$< 4\times10^{-3}$	5.1	6	< 0.01
Mn	—	—	$< 8\times10^{-3}$	1.8	< 1	< 0.01
Fe	< 0.007	< 1	< 0.02	5.0	3	0.04
Ni	—	—	< 0.3	11	< 1	0.14
Cu	—	—	< 20	1.8	< 1	0.33
Mo	—	—	$< 7\times10^{-5}$	0.6	< 1	< 0.01
Ag	—	—	—	76	< 1	0.82
Pt	—	—	—	< 0.5	< 1	< 0.01

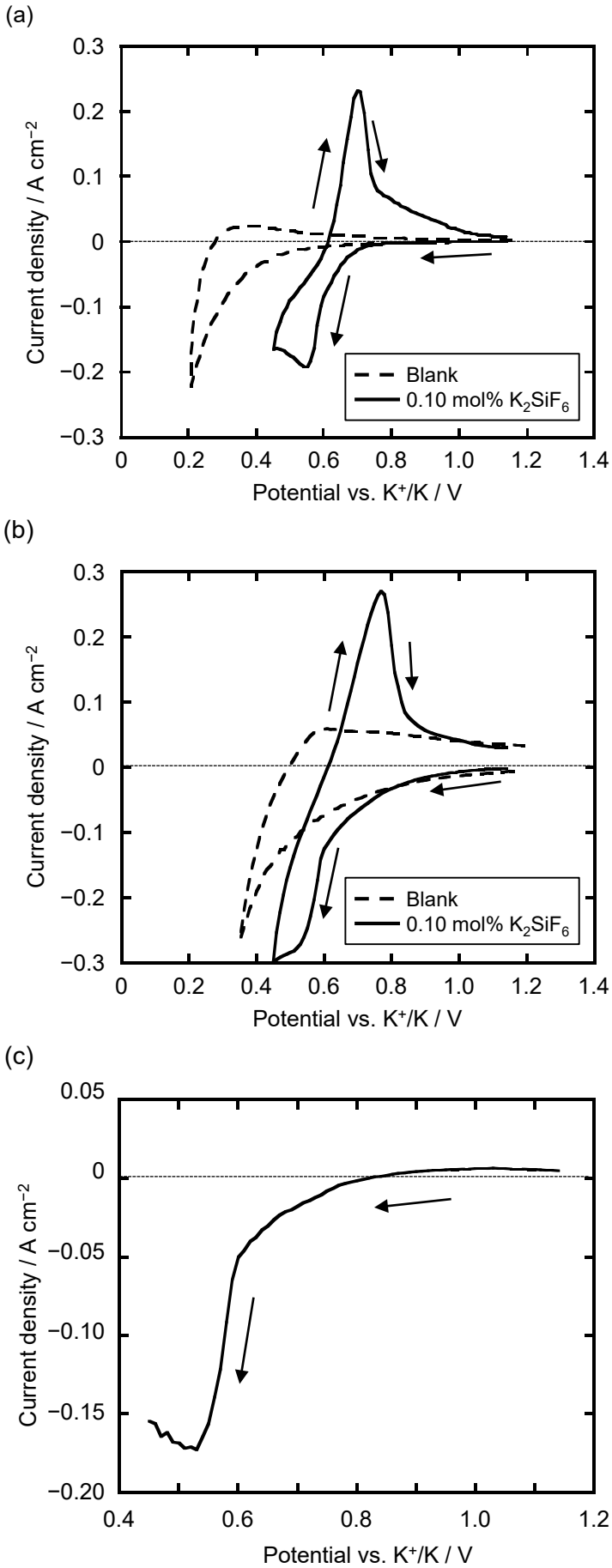

Fig. 1 Cyclic voltammograms at (a) a Ag flag electrode and (b) a graphite plate electrode in molten KF–KCl before and after addition of K_2SiF_6 (0.10 mol%) at 1073 K. Scan rate: 0.50 V s^{-1}. (c) Current–potential curve calculated from the difference for the voltammograms obtained at a graphite plate electrode in blank melt and molten KF–KCl−K_2SiF_6 (0.10 mol%).

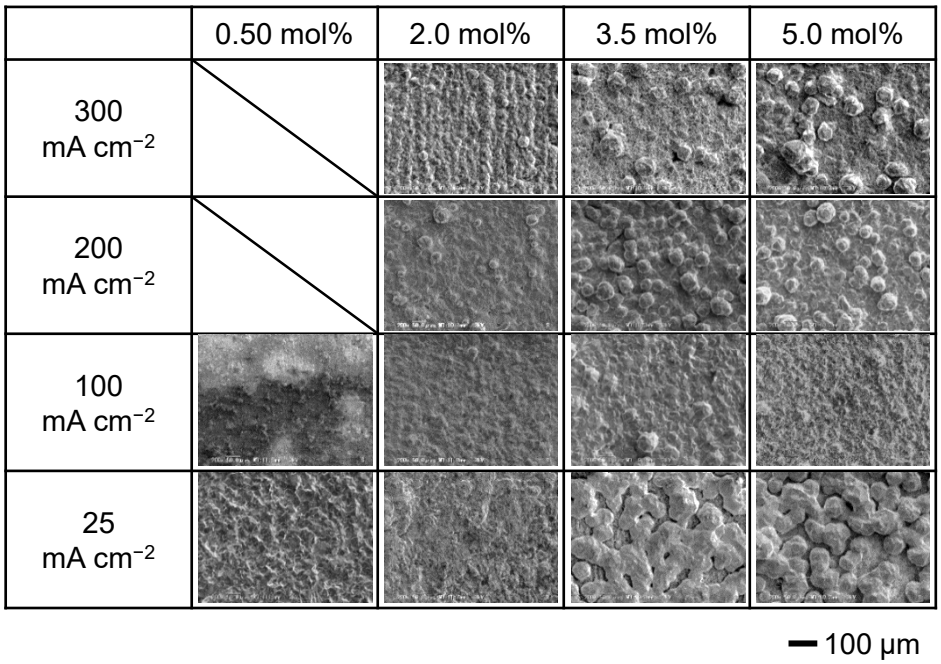

Fig. 2 Surface SEM images of the samples obtained by galvanostatic electrolysis of graphite plate electrodes at various current densities and K_2SiF_6 concentrations in molten KF–KCl at 1073 K. The charge density was 180 C cm^{-2}.

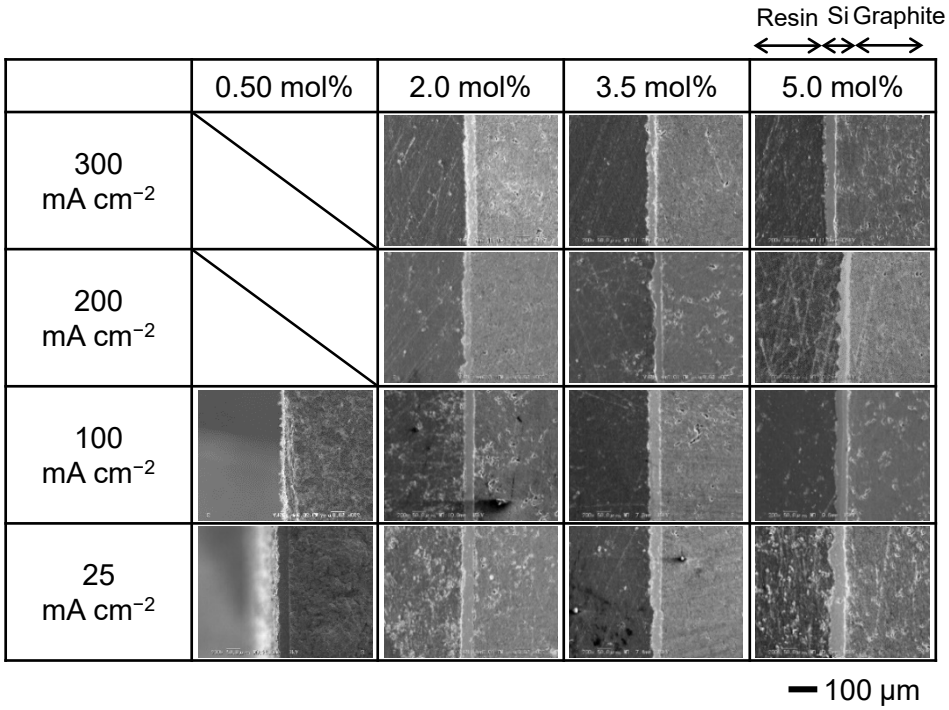

Fig. 3 Cross-sectional SEM images of the samples obtained by galvanostatic electrolysis of graphite plate electrodes at various current densities and K_2SiF_6 concentrations in molten KF–KCl at 1073 K. The charge density was 180 C cm^{-2}.

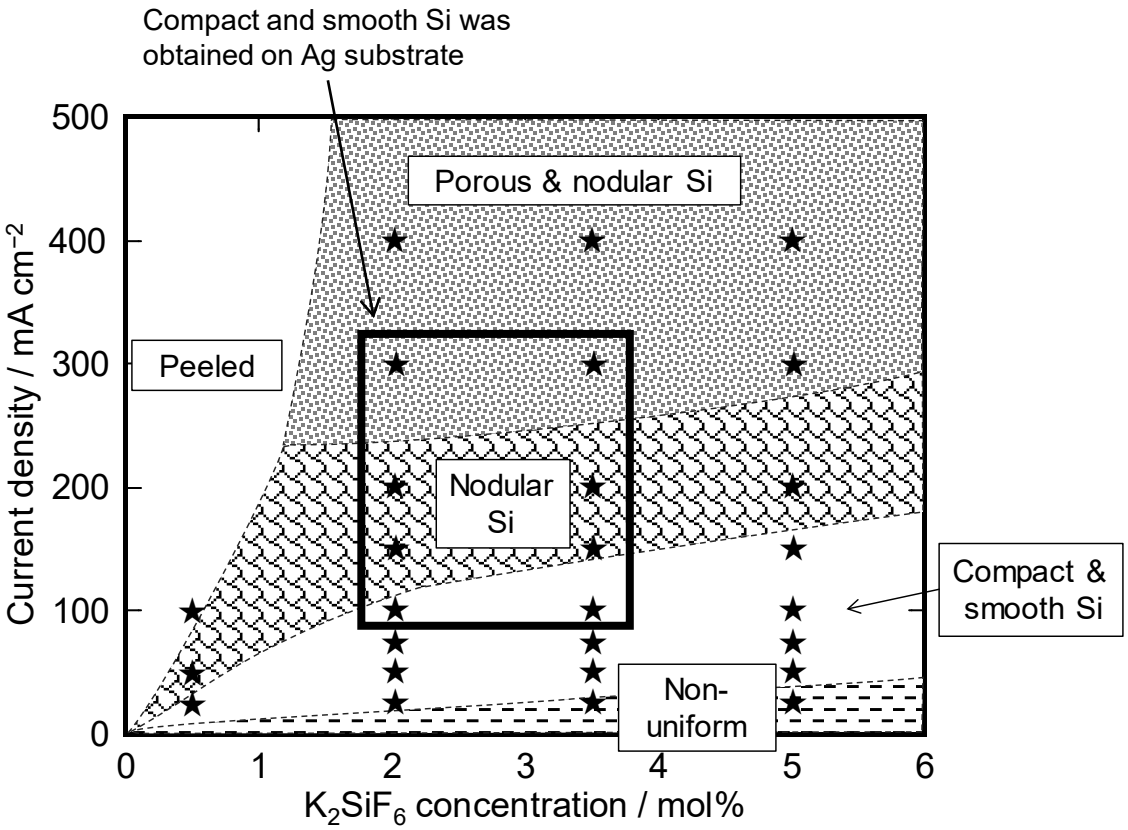

Fig. 4 Relationship between electrolysis conditions and morphology of Si deposits on graphite electrode and the optimum electrolysis conditions for Ag substrate [20].

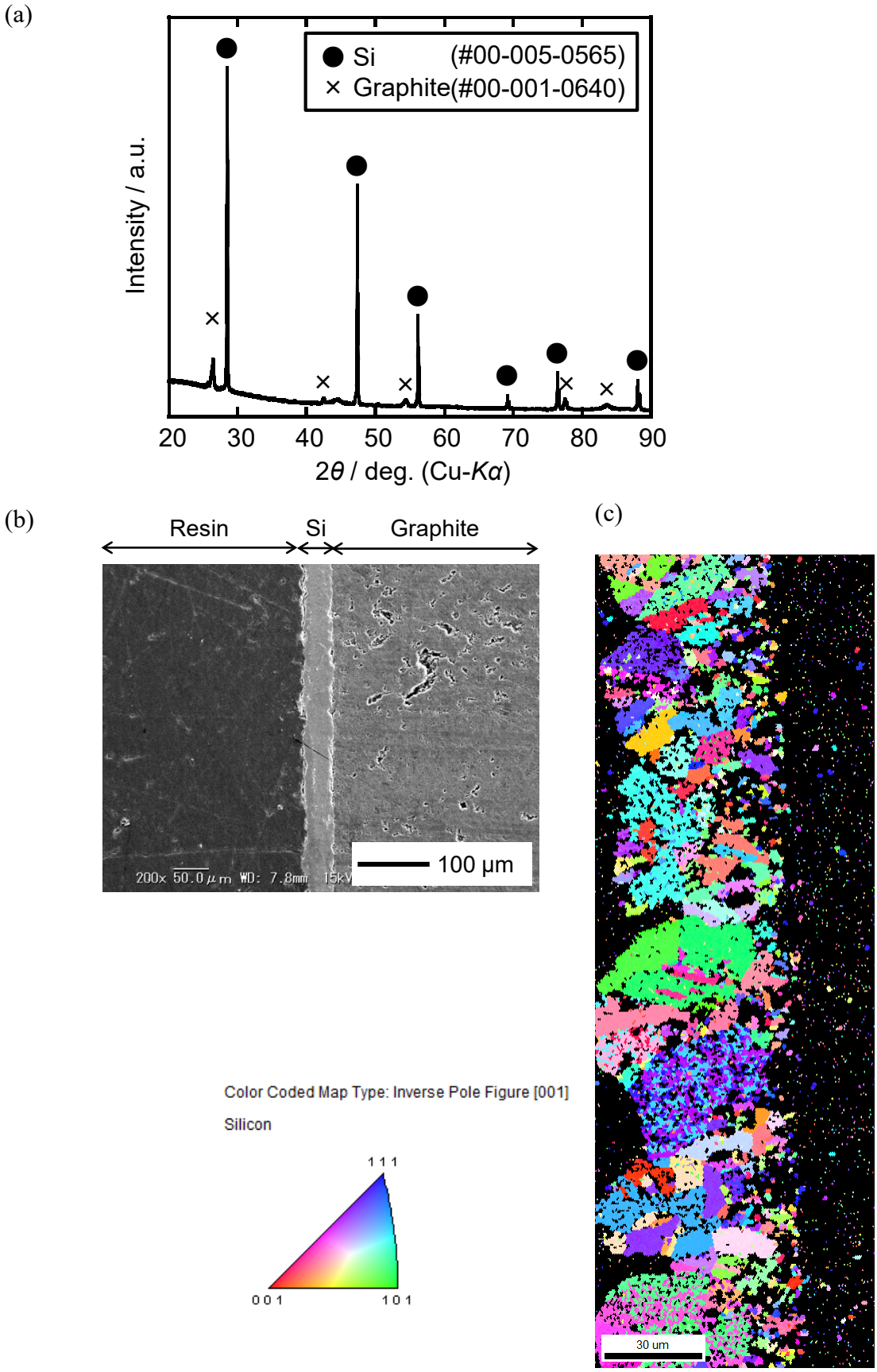

Fig. 5 (a) XRD pattern, (b) cross-sectional SEM image, and (c) a crystal grain map from electron backscatter diffraction (EBSD) analysis of the deposits obtained by galvanostatic electrolysis of a graphite plate electrode at 100 mA cm^{-2} for 30 min in molten KF–KCl–K_2SiF_6 (3.5 mol%) at 1073 K.

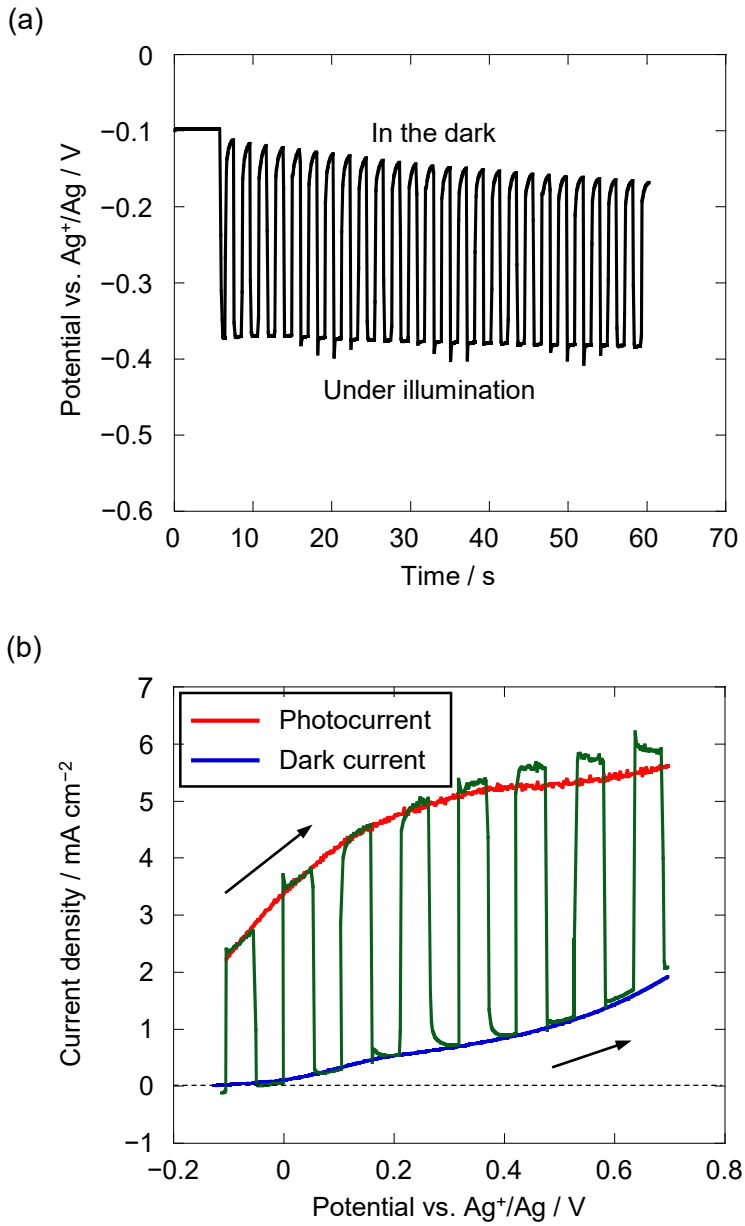

Fig. 6 (a) Open-circuit potentiogram and (b) linear sweep voltammograms at an electrodeposited Si in CH_3CN–$TBAPF_6$(0.1 M)–Fc(0.05 M) at room temperature. Scan rate: 0.05 V s^{-1}.

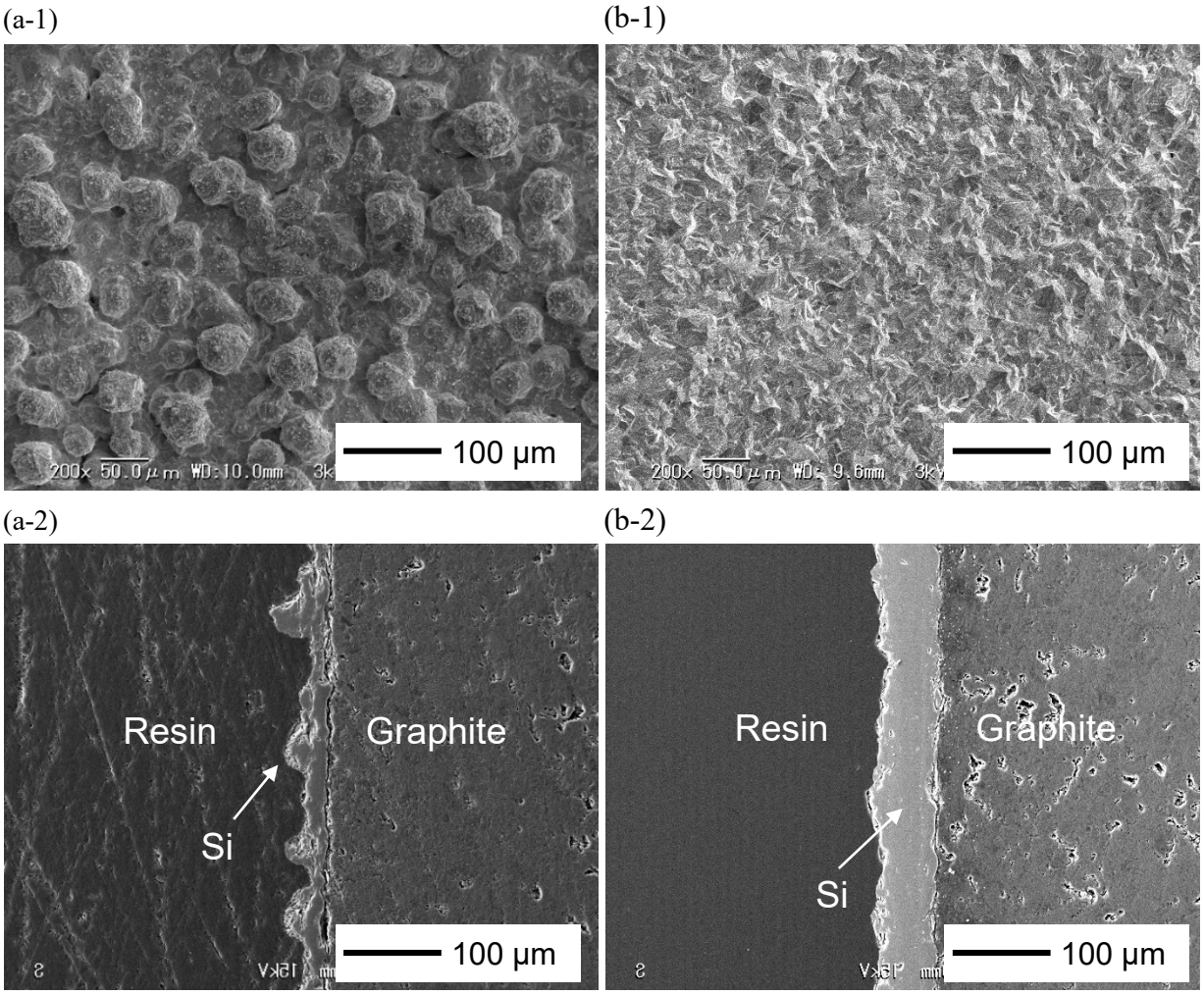

Fig. 7 Surface and cross-sectional SEM image of the samples obtained by galvanostatic electrolysis of graphite plate electrodes. The Si layer was electrodeposited (a-1)(a-2) at 100 mA cm^{-2} for 30 min in molten KF–KCl (45:55 mol%) at 1073 K after the introduction of $SiCl_4$ (2.79mol%) and (b-1)(b-2) at 45.6 mA cm^{-2} for 60 min in molten KF–KCl (60:40 mol%) at 1073 K after the introduction of $SiCl_4$ (2.37 mol%).

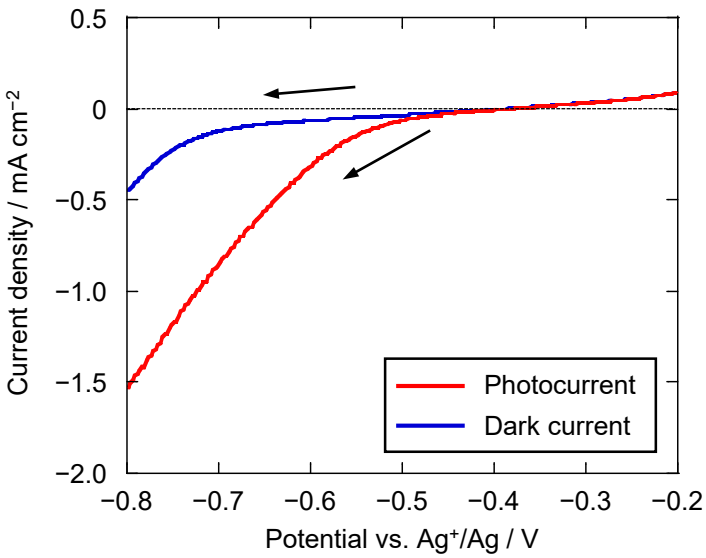

Fig. 8 Linear sweep voltammograms at the electrodeposited Si in CH_3CN–$TBAClO_4$ (0.3 M)–$EVBr_2$ (0.05 M) at room temperature. Scan rate: 0.05 V s^{-1}.